Engineered Science
DOI: https://dx.doi.org/10.30919/es1879

Dielectric Relaxation Behavior of Montmorillonite/Epoxy Resin Nanocomposites

Yujia Cheng, Lijie Peng and Guang Yu*

Abstract

Based on the research status of polymer matrix nanocomposite dielectrics, this study investigates the relationship between the interfacial structure of nanocomposites and their dielectric relaxation, polarization, and loss characteristics. Bisphenol-A epoxy resin (ER), commonly used as the primary insulation material in electrical equipment, served as the polymer matrix. A layered-silicate montmorillonite (MMT) served as the nanodispersed phase. MMT/ER nanocomposites were prepared via a melt-blending method. First, the formation mechanism of the nanocomposite interface was analyzed. In the composite system, electrostatic attraction occurs between the electronegative MMT layers and positively polarized centers of the ER polar dipoles, forming an two-phase interaction interface. Second, the effects of temperature and degree of resin cross-linking on the interface structure were analyzed. The nanocomposite interface morphology changed with increasing MMT content, which also influenced the dielectric polarization and loss characteristics. Finally, dielectric spectroscopy was performed on the MMT/ER nanocomposites to investigate the effect of the interface on their dielectric relaxation behavior under different MMT contents and frequencies.

Keywords: Dielectric relaxation behavior; Montmorillonite/epoxy resin nanocomposite; Dielectric polarization; Interface structure.
Received: 10 September 2024; Revised: 23 October 2025; Accepted: 09 November 2025
Article type: Research article.

1. Introduction

The concept of nanodielectrics was first proposed by Lewis *et al*., and correlational research in the field of nanodielectrics has been conducted for approximately 20 years.[1] However, the connection between performance and microstructure still remains unresolved.[2] The interface represents a unique structure within composites, and research on the interfacial structure and charge behavior plays a crucial role in understanding the relationship between nanodielectric structure and performance.[3] Increasing research-based results have highlighted the important role of the interface in determining macroscopic properties of nanodielectrics. Consequently, research based on the interface morphology, interface characteristics, and dielectric relaxation behavior is becoming increasingly detailed.[4]

The molecular structure of epoxy resin (ER) is stable even at high temperatures. The curing reaction can be completed using different curing agent compositions, and excellent performance can be achieved after the formation of a crosslinked structure.[5] Compared with other thermosetting resins that undergo polycondensation crosslinking, ER solidification does not produce water or other low-molecular-weight byproducts. Therefore, ER can effectively prevent air bubble formation during solidification.[6] This advantage is particularly evident when preparing ER composite samples, as porosity defects at the two-phase interface can be largely avoided, especially in ER composites used as main insulating materials.[7]

Montmorillonite (MMT) is a natural, inorganic silicate clay mineral with a lamellar nanostructure.[8] Structurally, MMT is a 2:1 type lamellar ionic crystal covalent compound, in which one aluminum oxide octahedral sublayer is sandwiched between two silicon-oxygen tetrahedron sublayers.[9] These sublayers are connected by covalent bonds that share oxygen atoms, and the unit cells are stacked parallel to each other.[10] Each lamella is approximately 1 nm thick and 100 nm wide, with an interlayer spacing of approximately 1 nm.[11] Within the lattice, isomorphous replacement of Al^{3+} and Si^{4+} ions occurs. Some aluminum ions in the aluminum oxide octahedral sublayer are replaced by low-valence ions, resulting in negatively charged lamellae. Free Na^{+}, Ca^{2+} and Mg^{2+} ions can substitute metal cations to balance the negative charge in the lamella.[12] The cell structure of the MMT

Mechanical and Electrical Engineering Institute, Zhongshan Institute, University of Electronic Science and Technology of China, Zhongshan, 528400, China
*Email: yuguang@zsc.edu.cn (Guang Yu)

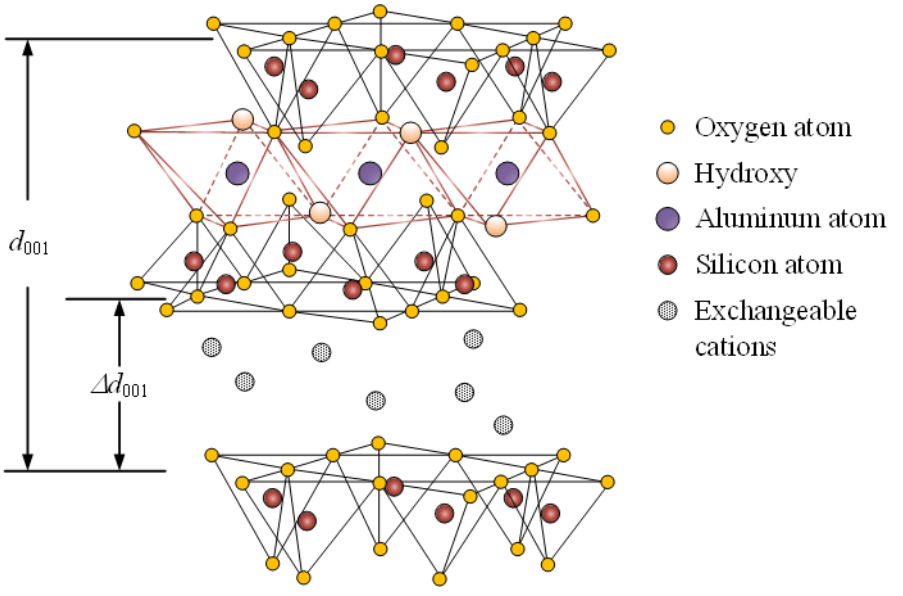

Fig. 1: Cell structure of a montmorillonite layer.

lamellae is shown in Fig. 1.

In general, the MMT lamellae are connected by weak electrostatic or van der Waals forces.[13] Under certain conditions, guest molecules can overcome these weak forces acting on the lamellae and be reversibly inserted into the interlayer gaps without destroying the lamellar structure.[14] The cohesive energy density of untreated MMT is typically high, resulting in poor compatibility with polymer surfaces.[15] In addition, the strong interlayer bonding interactions within the MMT lamellae hinder the insertion of polymer molecules, preventing effective composite formation.[16] Therefore, MMT must be organically treated before composite fabrication, allowing organic cations to replace the exchangeable cations in the lamella.[17] As a result, the surface properties of MMT change from hydrophilic to lipophilic. The organic modification process is illustrated in Fig. 2.

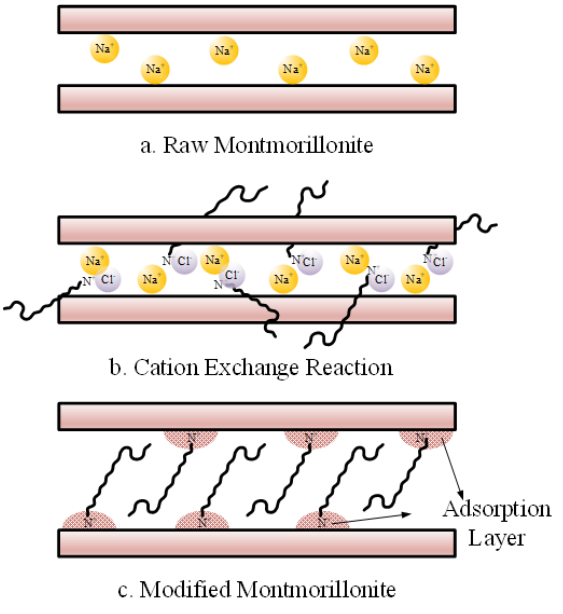

Fig. 2: Schematic showing the steps taken for modification of montmorillonite.

Numerous studies have reported that, after intercalation of MMT, the properties of MMT/ER nanocomposites improve compared with those of the pure ER matrix.[18] Although the causes of these property improvements have not been fully elucidated, they are believed to be related to changes in the mesoscopic structure of the nanocomposites. At present, research on mesoscopic structure is based on interface structure theory and several interface models.[19] Therefore, in this study, the process of interface formation in nanocomposites was investigated to analyze the interaction between the two phases at the interface.[20] The nanocomposites relaxation polarization and relaxation loss at different temperatures and frequencies were also examined. In addition, the effect of MMT content on the dielectric relaxation behavior was explored.[21] By combining studies on interfacial structure with those on dielectric relaxation behavior, the relationship between nanocomposites interfacial structure, dielectric relaxation polarization, and energy loss in nanocomposites can be elucidated.

2. MMT/ER nanocomposites samples preparation

The types of ER and curing agents used vary widely.[22] Depending on the combination of ER and curing agents, the ER solidifies with different properties. In this study, the most commonly used bisphenol-A ER, E-44, was used as a monomer. 3-MHHPA was used as a curing agent. Nano-MMT/ER samples were prepared using organically treated MMT. The skeleton formula of the E-44 monomer molecule is given below:[23]

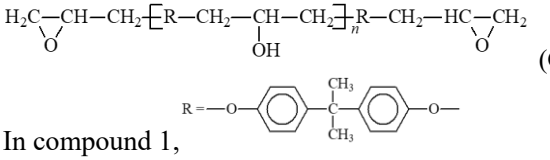

(Compound 1)

In compound 1,

The skeleton symbol of 3-MHHPA (Compound 2) is shown below.

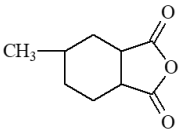

The measured amount of ER monomer was weighed and preheated to reduce its viscosity. After drying, the organic MMT was weighed according to the required mass ratio. The ER and MMT were directly mixed, and the temperature was maintained at a constant value. The blending process was carried out under low-viscosity conditions, which facilitate MMT dispersion in the resin. The mixture was stirred for a sufficient time to ensure uniform mixing. Because mechanical stirring introduces a large amount of gas into the melt, the temperature was maintained, and the melt was degassed until it became transparent.

At temperatures lower than the curing reaction temperature, the degassed melt was mixed with acid anhydride. The curing promoter was then added, and the mixture was stirred again until homogeneous. Subsequently, the pressure was reduced to extract residual air from the system. This process was repeated until no air bubble remained. Subsequently, the mixture was poured into a mold with a vacuum silicone grease and cured according to the precuring and curing procedures. Finally, after natural cooling and demolding, the nanocomposite samples were obtained. This process is shown in Fig. 3.

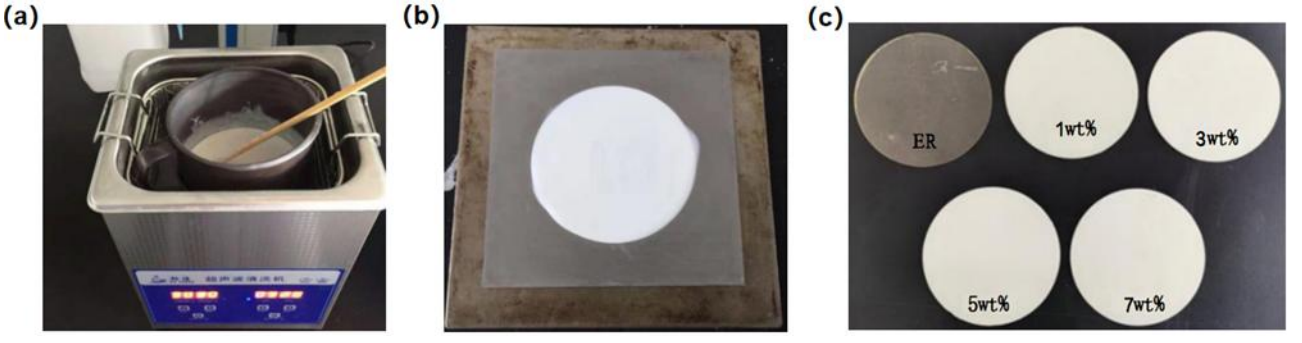

Fig. 3: (a) Ultrasonic oscillation (b) Sheeting (c) Different samples.

3. Results and discussion

3.1 MMT/ER nanocomposites relaxation polarization and loss

ER is a polar polymer present in various polymer materials.[24] Under an external electric field, the main types of polarization in the ER curing system are electronic displacement and dipole orientation polarization, with dipole orientation polarization being dominant. In MMT crystals, the main polarization mechanisms are electronic displacement, ionic elastic displacement, and thermion polarization. The electron cloud in the MMT lamella is constrained by the atoms at each node of the unit cell, resulting in synergistic binding effect.[25] Consequently, ionic elastic displacement polarization and thermion polarization dominate.

When ER and MMT are combined to form a composite, an interfacial layer is formed, controlling the polarization behavior of the composite system. In the MMT/ER composite, ER dipole orientation polarization, MMT lamella ionic elastic displacement polarization, and thermion polarization are often restricted by electrostatic interactions at the composite interface (Fig. 4); however, the exact underlying mechanism is difficult to understand.

Within the ER network, dipole orientation polarization is partially restricted by the crosslinked structure and mobility of molecular chain segments; however, dipole orientation polarization can still occur to some extent. In addition, the crystal lattice of MMT generates thermionic polarization under thermal motion, exhibiting relaxation polarization.[26] In the MMT/ER composite system, an interface-adsorbed layer is formed, as shown in Fig. 4. Electrostatic forces cause the two interfacial phases, unlike charge centers, to adsorb onto each other at the interface. This interfacial adsorption between ER and MMT phases impedes intrinsic polarization—dipole orientation polarization within ER and crystal lattice thermion polarization within MMT. In addition, the motion of dipole moments at the two ends of the interface is restricted by molecules from both ER and MMT phases, making polarization difficult to establish.

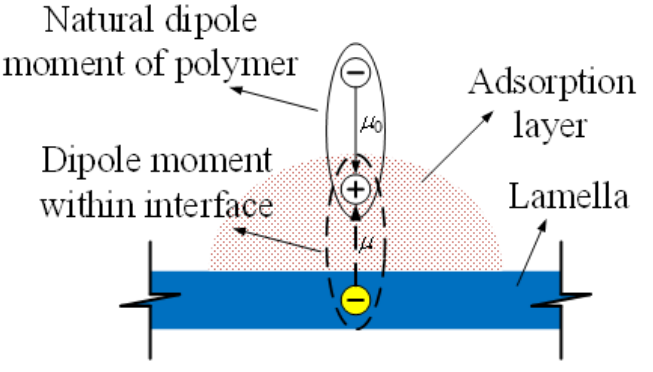

Fig. 4: Schematic diagram illustrating interfacial restriction to polarization.

When nano-MMT particles are added into an ER matrix, the decrease in overall composite polarization, contrary to the expected increase, can be attributed to the interfacial restriction on the intrinsic polarization within both phases. However, this restriction, which arises from the relaxation

polarization process, becomes more pronounced in nanocomposite systems. If the two phases fail to interact at the nanoscale, the ER molecules are unable to penetrate the MMT lamellae, leading to a reduced effective interfacial area within the composite.[27]

During polycondensation of ER with an acid anhydride, the MMT/ER nanocomposite interface is gradually developed as the system cures. Note that the mobility of polymer molecules varies with curing temperature; consequently, the thickness of the interfacial layer and the strength of interfacial adsorption also change, thereby affecting the polarization process within the nanocomposite system. Polycondensation reaction between ER and acid anhydride (curing agent) results in forming a crosslinked structure. The polycondensation reaction between ER and acid anhydride can be divided into two stages: precursor and curing. During the precursor stage, reaction occurs at low temperatures. During the initial phase of the curing stage, the acid anhydride initiates ER polymerization, forming polymerization centers and microgels within the ER monomer matrix. As the reaction proceeds, the sol proportion in the microgel system gradually decreases while the gel proportion increases, until a gel polymer network is formed. Interactions between gels are primarily governed by van der Waals forces. In this process, the MMT lamellae mainly interact with ER monomer molecules. The polycondensation of ER releases considerable heat, which gradually diffuses from the polymerization centers to the surrounding regions. The monomer molecules and MMT layers absorb this heat and exhibit enhanced thermal motion. Owing to the good compatibility between ER monomers and ammonium salts, the monomer molecules can penetrate the MMT lamellae and become adsorbed; however, this adsorption is unstable. The polymerization heat increases molecular mobility, making it is difficult for the monomers to remain stably adsorbed within the MMT layers. Compared with the crosslinked structure of the cured epoxy resin, the smaller monomer molecules can more easily penetrate the lamellae, allowing the layers to adsorb more monomer molecules. Consequently, the average interaction strength between the monomer molecules and the lamellae decreases, thereby reducing the electrostatic forces at the interface. The interfacial structure formed via this weak interaction is easily disrupted by molecular thermal motion.

During the precuring stage, a large number of ER monomer molecules are consumed, leading to microgel formation. These microgels undergo further curing at high temperatures to form crosslinked structures. As the curing of microgels progresses, a composite interfacial structure develops. As the monomer molecules gradually combine to form gels, their overall mobility decreases. Moreover, since the microgels are much larger than the monomer molecules, the amount adsorbed by the MMT lamellae is significantly lower. Consequently, the composite interface exhibits higher strength and tighter adsorption.

The pure ER, ER/raw MMT, and ER/organic MMT samples were prepared, and the relative dielectric constant (ε_r) and dielectric loss factor (tanδ) were measured at different temperatures to analyze the dielectric polarization process. The effect of the interfacial structure on polarization behavior was examined. The temperature-dependent variations of ε_r and tanδ for the three samples are shown in Figs. 5(a) and 5(b), respectively. As shown in Fig. 5(a), the ER/organic MMT exhibits the lowest dielectric constant. With increasing temperature, the growth rate of ε_r for ER/organic MMT decreases. Notably, both ER/organic MMT and ER/raw MMT exhibit higher ε_r values than that of pure ER, with the differences between ε_r values becoming particularly significant above 140 °C. As shown in Fig. 5(b), all samples exhibit an increase in tanδ values with temperature. In the 20–60 °C temperature range, the differences between tanδ values of the three samples are minimal. However, when the temperature exceeds 60 °C, these differences gradually become more pronounced. Among the examined samples, ER/organic MMT exhibited the lowest tan*d,* and ER/raw MMT exhibited the highest tanδ.

Based on the microstructural differences among the three

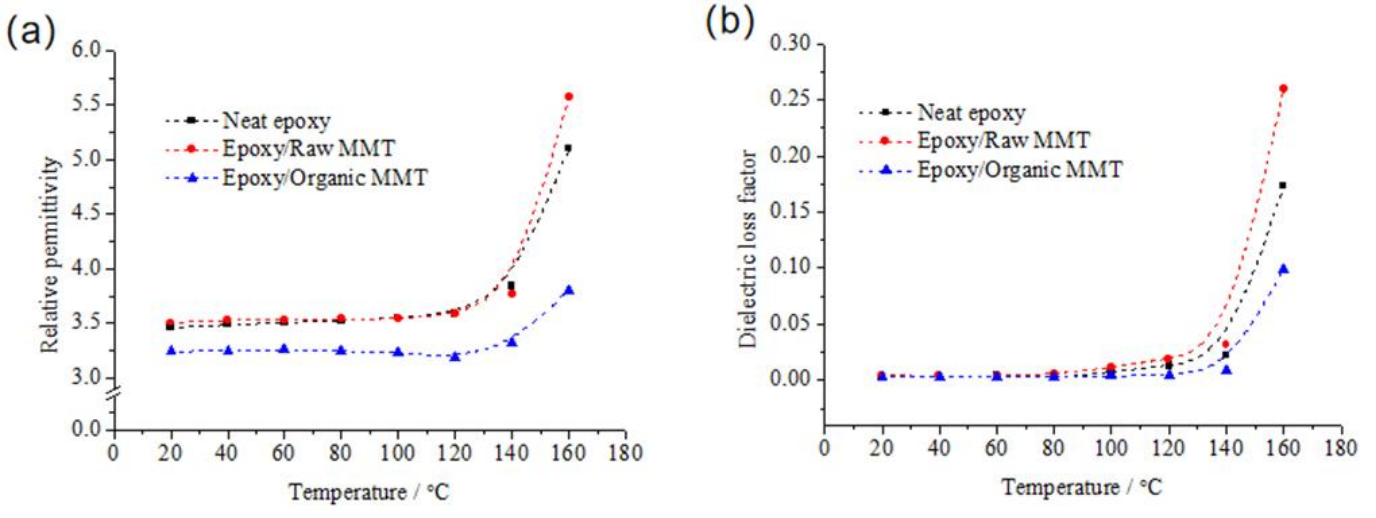

Fig. 5: Temperature dependence of (a) relative permittivity and (b) dielectric loss factor.

samples, the variations in dielectric constant and dielectric loss change can be attributed to different polarization behaviors. In pure ER, relaxation polarization arises mainly from dipole-orientation polarization in polar dielectrics. As the temperature increases, the thermal motion of molecules gradually becomes more pronounced. In the crosslinked structure of resin, freely movable molecular segments are limited by the crosslinked points. Consequently, the overall movement or orientation of the molecular segments is also restricted. Two types of molecular motions contribute to the establishment of dipole polarization in resin: (i) conformational changes within the molecular segments and (ii) restricted motion of local segments. The thermal motion of resin molecular segments improves with increasing temperature. At high temperatures, the resin molecules adsorb sufficient heat to overcome potential energy barriers, facilitating local conformational and orientational changes in the molecular segments and increasing the number of polarized molecular dipoles. When an electric field is applied, these dipoles align along its direction. Consequently, the number of dipole moments per unit volume in the direction the electric field increases, resulting in an increase in the relative dielectric constant.

Compared with the original three-layer structure of MMT, the interlayer spacing of MMT increases after organic modification. The slight difference in compatibility between ER monomer molecules and MMT lamellae restricts the ER monomer molecules from penetrating the MMT lamellae, leading to the formation of a composite interface. When ER monomer molecules initiate polymerization within the MMT lamellae, an organic phase develops inside the lamellae, resulting in the formation of an interfacial region. In ER/organic MMT, interfacial adsorption occurs between the resin matrix and MMT lamellae. At the MMT/ER interface, the motion of molecular segments or lattice atoms in both phases is restricted. Under a low electric field strength (1×10^6 V/m), the interfacial electrostatic attraction is ~10^3 times stronger than the applied electric field force, making it difficult for dipoles to align along the field direction. Consequently, relaxation polarization weakens, leading to a decrease in the relative dielectric constant.

Notably, in ER/raw MMT, the MMT and ER matrices do not form nanocomposites, and the MMT nanoparticles remain dispersed as clusters in the ER matrix. A composite interface that restricts the motion of molecules or lattice atoms between the two phases does not form. In addition to the orientation polarization of resin molecular dipoles, thermionic polarization of MMT crystals occurs. Consequently, the dielectric relaxation, polarization, and loss increases, particularly at high temperatures.

For comprehensive performance index evaluation of the curing system, the precuring temperature of ER was set to 90 °C. The pure ER samples were subsequently cured at 120, 150, and 180 °C for 6 h. The variation curves of the composites ε_r and tanδ with temperature are shown in Figs. 6(a) and 6(b), respectively.

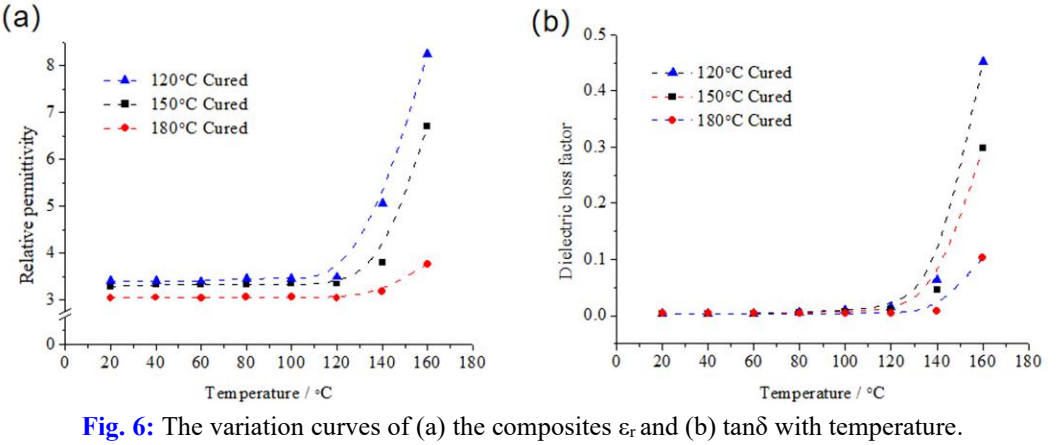

Fig. 6: The variation curves of (a) the composites ε_r and (b) tanδ with temperature.

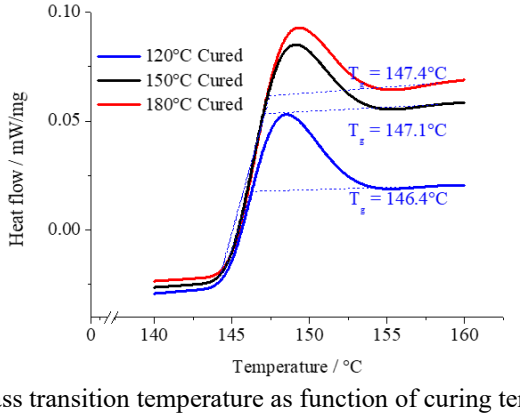

Fig. 7: Glass transition temperature as function of curing temperature.

Next, DSC was performed on the MMT/ER composites. The glass transition temperature was selected based on the ER curing process at different curing temperatures, and the DSC results are presented in Fig. 7. The relaxation polarization derived from the temperature dependence of the ε_r and tanδ directly reflects the variation in molecular mobility across different samples. Based on the differences in the glass transition temperatures after a 6 h curing process at different temperatures, the ER curing reaction was considered complete. All samples exhibited comparable glass transition temperatures. The glass transition temperature of the sample cured at 120 °C was slightly lower than those of the samples cured at 150 °C and 180 °C. All three examined samples transformed into microgels by the end of the precursor stage. During curing at different temperatures, chemical bonds connecting the molecular chains are formed within the microgels. Subsequently, a crosslinked structure is established. Notably, the sample cured at 120 °C exhibited a lower crosslinking density and fewer crosslinking points, with relatively long molecular segments between the crosslinked points. The molecular segments exhibited a certain degree of mobility. Under the same interfacial adsorption conditions, the molecular segments exhibited relatively higher mobility that allowed them to escape easily from the interfacial layer, marking the completion of the relaxation transition process. In contrast, at the composite interface between the highly crosslinked ER matrix and MMT, the mobility of the molecular segments was considerably reduced, even under the same interfacial binding effect. As a result, internal conformational retations or local segmental reorientations became difficult to achieve. Owing to the restrictive influence of the interfacial layer, relaxation polarization was significantly hindered.

As shown in Fig. 6(a), the ε_r values of the composites are inversely proportional to the curing temperature in the range of 20–160 °C. In the low-temperature-cured samples, restricting the molecular motion during interfacial adsorption was difficult. Dipole orientation polarization could be achieved to a certain extent. Therefore, the low-temperature-cured samples exhibited a large e_r. As the curing temperature increased, the crosslinking density in the ER matrix gradually increased. The molecular segments between the crosslinked points shortened, and the mobility of the molecular segments weakened. Interface-layer adsorption restricted the steering motion. The ε_r value was lower, particularly at high temperatures. As the temperature exceeded the glass transition temperature, the mobility of the molecular segments improved significantly in the low-temperature-cured samples. Dipole orientation polarization was more easily established. At high temperatures, the polymer molecular segments successfully overcame the mobility restriction imposed by the interfacial layer. The binding effect of the interfacial layer on MMT thermionic polarization was also alleviated. Consequently, the ε_r value increased significantly. In contrast, the high-temperature-cured samples exhibited a relatively higher crosslinking density of the molecules. The mobility of the molecular segments was limited, and interface layer adsorption could not be eliminated. Steering of the polymer molecular segments was restricted by the interface layer, which also limited the thermionic polarization in the MMT lamella. The overall ε_r value was small. In addition, the fully crosslinked structure restricted the mobility of the molecular segments. At high temperatures, the mobility of the molecular segments did not improve significantly, and the mobilities of the molecular segments and MMT lamellae remained restricted by the interfacial layer. The ε_r value changed only slightly. Similarly, the tanδ and relaxation loss of three examined samples showed no significant change with increasing temperature in the range of 20–60°C. With increasing temperature, the molecular segments in the low-temperature-cured samples possessed a certain degree of mobility. Interface layer adsorption did not restrict the establishment of the relaxation polarization process, and the relaxation loss also increased. When the temperature reached 100 °C, the relaxation loss in low-temperature-cured samples increased significantly. The higher the temperature, the larger was the relaxation loss. An increase in the number of mobile molecular segments helped eliminate interface restrictions, and the relaxation loss increased rapidly. During this temperature variation process, the relaxation loss in the high-temperature-cured samples remained at a lower level. Considering the conductive loss induced by exogenous impurity ions, when the temperature reached 160 °C, the loss increment exhibited by the high-temperature cured samples was much smaller than that exhibited by the low-temperature cured samples.

3.2 Effect of MMT content on composites dielectric relaxation

As nano-MMT content increases in an MMT/ER nanocomposite, the interfacial structure between the two components gradually develops and expands. The composite interface restricts relaxation polarization in both phases. As the proportion of the interfacial structures increases, a greater number of resin molecules are restricted from infiltrating the MMT layer. Consequently, the number of relaxation-polarizable molecules per unit volume decreases and, in turn, polarization intensity also decreases. As the MMT concentration is further increased, the probability of MMT particle collisions during dispersion also increases, resulting in aggregation of nano-MMT particles forming microscale clusters. Consequently, the effective proportion of the nanocomposite interfacial structure decreases. The surface energies of these micro-MMT clusters are considerably lower than those of dispersed nano-MMT particles, leading to a weakened two-phase interfacial binding effect. Under such conditions, the relaxation polarization of resin molecules and MMT particles can be more readily established.

At a constant temperature, the dielectric frequency spectra of the composites were measured to characterize the

composite relaxation polarization process. Based on the distribution of polymer relaxation times, the Debye equation without conductance can be modified, and the composite dielectric constant is given by:

$$\varepsilon^* = \varepsilon_\infty + \frac{\varepsilon_s - \varepsilon_\infty}{1+(i\omega\tau)^{1-\alpha}} \quad (1)$$

where a represents the relaxation time dispersion. A smaller a value corresponds to a narrower the relaxation time distribution. If $a = 0$, the dielectric exhibits a single relaxation time. Eq. 1 can be expressed in trigonometric form, giving the real (ε′) and imaginary (ε″) parts of the complex dielectric constant as follows:

$$\varepsilon' = \varepsilon_\infty + (\varepsilon_s - \varepsilon_\infty)\frac{1+(\omega\tau_0)^{1-\alpha}sin\frac{\pi\alpha}{2}}{1+2(\omega\tau_0)^{1-\alpha}sin\frac{\pi\alpha}{2}+(\omega\tau_0)^{2(1-\alpha)}} \quad (2)$$

$$\varepsilon'' = (\varepsilon_s - \varepsilon_\infty)\frac{(\omega\tau_0)^{1-\alpha}cos\frac{\pi\alpha}{2}}{1+2(\omega\tau_0)^{1-\alpha}sin\frac{\pi\alpha}{2}+(\omega\tau_0)^{2(1-\alpha)}} \quad (3)$$

In Eqs. 2 and 3, ε′ and ε″ can be regarded as the reactive and active components, respectively. These can be transformed into Eq. 4:

$$tan\delta = \frac{\varepsilon''}{\varepsilon'} \quad (4)$$

When $\omega\tau_0$ in Eqs. 2 and 3 is eliminated, Eq. 5 is obtained:

$$\left[\varepsilon' - \frac{(\varepsilon_s+\varepsilon_\infty)}{2}\right]^2 + \left[\varepsilon'' + \frac{(\varepsilon_s-\varepsilon_\infty)}{2}\tan\frac{\pi\alpha}{2}\right]^2 = \left[\frac{(\varepsilon_s-\varepsilon_\infty)}{2}\frac{1}{\cos\frac{\pi\alpha}{2}}\right]^2 \quad (5)$$

Using the relative dielectric constant and loss measured at different frequencies, a values of the samples at a given test temperature can be calculated using Eqs. 1 to 5. The ε_r and tanδ values of nano-MMT/ER composites with 1%, 3%, 5%, and 7% MMT contents at room temperature are shown in Figs. 8(a) and 8(b), respectively. The calculated a values for the composites are listed in Table 1.

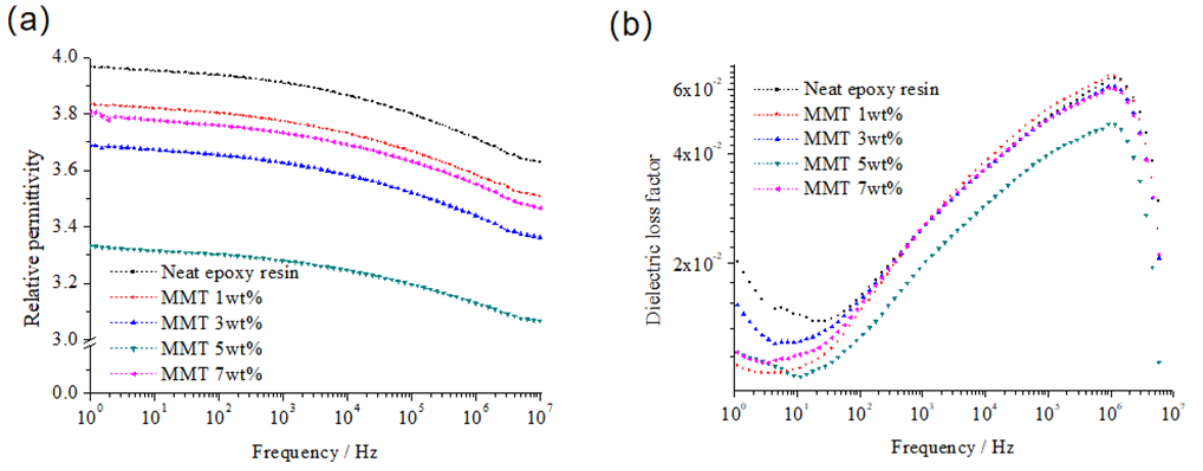

Fig. 8: Frequency dependence of (a) relative permittivity and (b) dielectric loss factor with varying MMT content.

Table 1: Values of ε_s, ε_∞, $\varepsilon_s-\varepsilon_\infty$, and a for MMT/ER nanocomposites with different MMT contents.

MMT content/wt%	ε_s	ε_∞	$\varepsilon_s-\varepsilon_\infty$	α
0	3.99	3.51	0.48	0.748
1	3.83	3.43	0.4	0.713
3	3.75	3.35	0.4	0.726
5	3.33	3.03	0.3	0.697
7	3.78	3.42	0.46	0.718

The results shown in Fig. 8(a) indicate that ε_r gradually decreases with increasing temperature for all samples. This indicates that the dielectric polarization process in the composites follows the same relaxation mechanism as in pure ER. The process corresponds to a typical relaxation behavior. Furthermore, the response range of tan$d$ and the peak frequencies are identical across all samples, indicating that no new type of polarization occurs.

After the composite interface between the dispersed MMT phase and the resin matrix is formed, the steering motion of resin dipoles in the interfacial region is restricted. Consequently, polarization cannot be fully established. In contrast, in the non-interfacial region, the resin molecular segments are only slightly affected by the composite interface. At an appropriate frequency, dipole steering polarization can still be established. In addition, the a of the molecules in the non-interfacial region is identical to that of the pure ER molecules. Note that a is related to an action unit that varies in size. Therefore, the polymer relaxation process is represented by a distribution function that exhibits polydispersity.

Considering that only a few side groups or branched chains are present in the ER main chains, large rigid branched chains

are almost entirely formed via monomer condensation. Notably, cured ER has a crosslinked structure, with molecular chain motions restricted at crosslinked points. Polarization establishment relies mainly on polar segments within parts of the molecular main chains. The main relaxation process is the *g*-secondary relaxation of the molecular segments.

At the composite interface, two-phase adsorption restricts the establishment of relaxation polarization in the respective system. Only local segments with weak mobility can form a stable interface with the MMT lamellae. In the ER-cured nanocomposite system, ER matrix molecules form a crosslinked structure after the curing reaction, resulting in loss of mobility of the entire molecular segment. The ER-cured nanocomposite systems exhibit relatively large *a* values, and even at high temperatures, whole-chain molecular motion does not occur in these systems. Moreover, *a* level relaxation is also not established for such systems. In conclusion, the resin relaxation time depends only on mobility of local segments in resin molecules.

After formation of the composite interface, the absorbed resin molecules cannot undergo *g*-secondary relaxation, and the resin molecules outside the composite maintain their mobility. Therefore, the *g*-secondary relaxation time does not significantly change. However, the relaxation time distribution can still be affected. Without restriction from the composite interface, various movable groups or local segments in the resins can establish polarization. At this point, the *a* reaches its maximum. If not all relaxation in the resin be established, the resin exhibits a single relaxation time that approaching infinity, with $a = 0$. The higher the proportion of the effective composite interface, the more restricted is the relaxation process of resin molecules, preventing the establishment of the *g*-secondary relaxation process.

The values listed in Table 1 indicate that *a* first decreases and then increases with increasing MMT content in the MMT/ER nanocomposites. When the MMT content reaches 5wt%, *a* decreases to its lowest values, indicating that the effective composites interface ratio of 5wt% nano-MMT/ER is the highest. At 5wt% MMT, the MMT/ER nanocomposite exhibits heterogeneous medium adsorption, promoted by the effective dispersion of MMT nanoparticles in the resin matrix. In other examined nanocomposites, the collision probability among MMT nanolayers increases, leading to aggregation of nano-MMT particles and a decrease in the interface ratio. When the MMT content reaches 7wt%, the ε_r and tanδ values of nano-MMT/ER are lower than those of pure ER. Although some nano-MMT particles aggregate, effective nanocomposites interfaces are still formed. MMT aggregation can be observed in the cross-sectional SEM images (Figs. 9(a) and 9(b)) of the nano-MMT/ER composites containing 5wt% and 7wt% MMT. SEM imaging revealed that at 5wt% MMT, the MMT nanoparticles form layered dispersion in the resin matrix, whereas at 7wt% MMT, the MMT lamellar structure is still present but the nanoparticles dispersed in clusters.

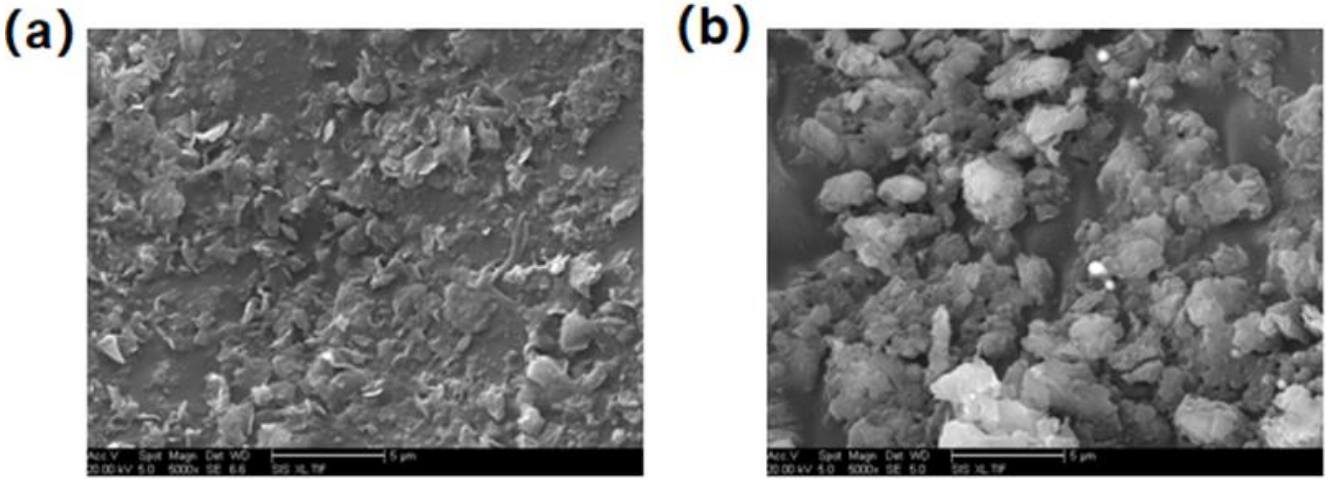

Fig. 9: Cross-sectional SEM images of the nano-MMT/ER composites containing (a) 5wt% and (b) 7wt% MMT.

In Fig. 9(a), only one loss peak is observed in the composites and pure ER samples in the frequency range of 1–10^7 Hz. Although all samples exhibit different values of tan*d*, their response frequencies corresponding to the loss peaks are identical, suggesting that Maxwell–Wagner interfacial polarization may exist in the nanocomposites. However, interfacial polarization is not observed in the frequency range of 1–10^7 Hz. Interfacial polarization occurs in heterogeneous dielectrics composed of components with different relative dielectric constants or conductivities. Under an external electric field, the aggregation of electrons or ions at the interface induces interfacial polarization. For nanocomposites, at normal temperatures and low testing voltages, the dielectric conduction is mainly ionic, and intrinsic ionic or electronic conductance is difficult to achieve. The ions responsible for conduction in MMT/ER composites are mainly exogenous impurity ions and/or weakly bound ions in MMT particles. Under an applied electric field, the average carrier mobility is low. Compared to electrons, ions are less likely to be captured by dielectric traps, making the accumulation of partial electric charge difficult. Under alternating electric fields in the frequency range of 1–10^7 Hz, ion carriers hardly migrate to the

composite interface or accumulate. Therefore, in the tested frequency range, dielectric loss can be attributed mainly to relaxation polarization, and no new type of polarization is observed in the dielectric.

4. Conclusion

In nano-MMT/ER composites, a two-phase composite interface is formed due to electrostatic adsorption between the electropositive organic phase and the electronegativity of the inorganic phase. To a certain extent, the movement of molecules or ions in this two-phase composite system is restricted. The main findings of this study are summarized as follows.

According to the XRD and FTIR results, the organic modification of MMT improved the microenvironment of the laminates, enabling easier insertion of ER molecules into the laminates and the formation of nanocomposites. SEM and TEM results visually confirmed the two-phase composite structure. After curing, the intercalation of ER molecules into the MMT produced exfoliated nanocomposites. The intrinsic grain-cluster structure of MMT was disrupted and dispersed homogeneously across the ER matrix, displaying a layered morphology.

The formation mechanism of the composite interface was attributed to electrostatic adsorption between the two phases. Two factors influencing the interface structure were investigated: the molecular polarity and composite temperature of the organic phase. The polarity of the organic phase facilitates electrostatic adsorption on the MMT layers. However, the repulsive force among the lattice ions in the MMT layers decreased because of the strong electrostatic attraction, weakening the diffusion of the adsorption layer at the interface and consequently reducing the interface area. In contrast, when a nonpolar polymer interacts with MMT layers, the electrostatic adsorption capacity between the two phases is weak, increasing molecular repulsion in the MMT layers. This reduces the cohesive energy density and increases the surface atomic potential energy. The surface atoms the undergo diffusion adsorption, which compensates for the bond energy of the outward-pointing atoms, allowing diffusion of the composite interface adsorption layer. At high temperatures, both the polymer molecules and MMT ionic layers exhibit strong molecular motion, making stable electrostatic adsorption difficult to establish between the two phases. This is unfavorable for interface formation. Conversely, at lower temperatures, the reduced thermal motion of molecules facilitates electrostatic equilibrium, promoting interface formation. However, when the temperature is too low, the polar groups of the polymer molecules are often coated or entangled with molecular chains, leading to conjugation or steric hindrance that may weaken the molecular polarity of the polymer. Additionally, if the electropositive atoms or groups are completely shielded, electrostatic attraction with MMT layers cannot. The organic and inorganic phases exhibit a mutual binding effect at the interface, restricting the dipole orientation polarization of ER molecules and thermion polarization of the MMT layers. The adsorption layer at the interface moderately limits molecular motion. When the mutual binding effect among polymer molecular segments weakens, the molecules disrupt the electrostatic adsorption at the interface through their thermal motion, completing the relaxation transition.

For the ER resin with a crosslinked structure, the main relaxation process is *g*-secondary relaxation of molecular segments. The interface does not change the composite polarization type but restricts the establishment of *g*-relaxation process in local segments. Consequently, the ε_r and tanδ values of the composite samples decrease. However, the polarization of the composites remain a relaxation process. Under alternating electric fields in the frequency range of 1–10^7 Hz, interfacial polarization was not observed; it appeared only at lower frequencies. With increasing MMT content, MMT tends to reunite the composites. When the MMT content was below 5wt%, the MMT maintained a laminar dispersion in the ER matrix, contributing to effective nanocomposite interface formation. When the MMT content exceeded 5wt%, the nano-MMT layers mutually adsorbed and formed micro-agglomerate particles, decreasing the effective interface area of the nanocomposites.

Acknowledgments

This research was aided by the key area campaign of regular universities in Guangdong province (Nos. 2021ZDZX1058 and 2024ZDZX4074), Guangdong Basic and Applied Basic Research Foundation (Nos. 2025A1515010595 and 2023A1515240063).

Conflict of Interest

There is no conflict of interest.

Supporting Information

Not applicable.

CRediT Statement

Yujia Cheng: Writing - Review & editing, Supervision, Resources, Project administration, Investigation, Supervision, Software. **Lijie Peng:** Writing - Original draft, Methodology, Investigation, Formal analysis, Data curation. **Guang Yu:** Writing – Review & editing, Funding acquisition, Supervision, Resources.

References

[1] Y. R. Kumar, K. Deshmukh, J. Kadlec, S. K. Khadheer Pasha, Dielectric properties of nano-MMT and graphene quantum dots embedded poly (vinylidene fluoride-co-hexafluoropropylene) nanocomposite films, *Journal of Applied Polymer Science*, 2023, **140**, e53724, doi: 10.1002/app.53724.

[2] V. J. Vipu Vinayak, K. Deshmukh, M. Pandey, S. K. Jameer

Basha, P. N. Muskawar, V. R. K. Murthy, S. K. Khadheer Pasha, Synergistic effect of nano-$BaTiO_3$ and montmorillonite nanoclay on the AC conductivity and dielectric properties of poly(vinylidenefluoride) nanocomposite films, *Ferroelectrics*, 2024, **618**, 561-575, doi: 10.1080/00150193.2023.2273732.

[3] J. Hu, X. Zhao, J. Xie, Y. Liu, S. Sun, Influence of organic Na^+-MMT on the dielectric and energy storage properties of maleic anhydride-functionalized polypropylene nanocomposites, *Journal of Polymer Research*, 2022, **29**, 182, doi: 10.1007/s10965-022-03047-w.

[4] N. Gürler, G. Torğut, Physicomechanical, thermal and dielectric properties of eco-friendly starch-microcrystalline cellulose-clay nanocomposite films for food packaging and electrical applications, *Packaging Technology and Science*, 2022, **35**, 473-483, doi: 10.1002/pts.2643.

[5] R. J. Sengwa, C. P. Charan, Characterization of MMT and OMMT nanofillers effect on the optical, dielectric, electrical, and electrochemical properties of PEO/PMMA/P(VDF-HFP)/LiTFSI solid polymer electrolytes, *Polymer-Plastics Technology and Materials*, 2025, **64**, 2735-2748, doi: 10.1080/25740881.2025.2562428.

[6] Y. Cheng, G. Yu, Effects of varying nano-montmorillonoid content on the epoxy dielectric conductivity, *Molecules*, 2024, **29**, 4650, doi: 10.3390/molecules29194650.

[7] P. Rani, S. K. Khadheer Pasha, A study of EMI shielding efficiency, dielectric, and impedance properties of polymer nanocomposites reinforced with Graphene nanoplatelets, montmorillonite, and copper oxide nanoparticles, *Polymer-Plastics Technology and Materials*, 2024, **63**, 2258-2275, doi: 10.1080/25740881.2024.2369680.

[8] M. Dehghani-Dashtabi, H. Hekmatara, M. Mohebbi, Tuned decoration of sodium montmorillonite (Na-MMT) nanoclay with $MoSe_2$/RGO for enhancing microwave absorption, *Scientific Reports*, 2025, **15**, 28731, doi: 10.1038/s41598-025-14387-0.

[9] S. Li, G. Zheng, C. Cao, C. Zhu, B. Zhang, Z. Cai, P. Feng, Interfacial engineering of hydrophobic montmorillonite for high-energy-capability polypropylene nanocomposite dielectrics, *Crystals*, 2025, **15**, 786, doi: 10.3390/cryst15090786.

[10] R. J. Sengwa, P. Dhatarwal, PVA/MMT and (PVA/PVP)/MMT hybrid nanocomposites for broad-range radio frequency tunable nanodielectric applications, *Materials Letters*, 2021, **299**, 130081, doi: 10.1016/j.matlet.2021.130081.

[11] G. Torğut, N. Gürler, Nanofiller reinforced biodegradable PHA/PLA composites: physico-chemical, thermal and dielectric properties, *Journal of Polymer Research*, 2021, **28**, 452, doi: 10.1007/s10965-021-02816-3.

[12] L. Ben Ammar, H. Hammami, S. Fakhfakh, S. Taktak, Impact of nanoclay loading on the structural, thermal and dielectric properties of montmorillonite/polypropylene nanocomposites, *Polymer Composites*, 2021, **42**, 2492-2501, doi: 10.1002/pc.25994.

[13] J. Gao, Z. Yao, L. Liu, H. Ju, L. Li, N. Guo, J. Niu, The effect of polyethylene-based nano-montmorillonite composite interfaces on charge transport, *Journal of Materials Science: Materials in Electronics*, 2023, **34**, 860, doi: 10.1007/s10854-023-10268-2.

[14] A. K. Nath, B.Sharma, B. J. Borah, N.Deka, J.Hazarika, Structural and electrochemical properties of montmorillonite-poly(ethylene oxide) intercalated nanocomposites for lithium-ion batteries, *International Journal of Polymer Analysis and Characterization*, 2023, **28**, 279-291, doi: 10.1080/1023666X.2023.2207867.

[15] Z. Hou, S. E. Chavez, A. M. LaChance, M. D. Jones, C. D. French, A. M. Walsh, M. T. Shaw, L. Sun, Polyvinyl alcohol (PVA)/montmorillonite (MMT) nanocomposite coatings *via* a rotational coating method, *Advanced Composites and Hybrid Materials*, 2024, **7**, 150, doi: 10.1007/s42114-024-00965-9.

[16] T. Yang, C. Wang, L. Liu, L. Zhang, Silicone elastomer dielectric composites by introducing novel O-MMT@TiO_2 nanoparticles for energy harvesting application, *Composites Part A: Applied Science and Manufacturing*, 2024, **185**, 108351, doi: 10.1016/j.compositesa.2024.108351.

[17] M. Lahbib, C. Mejri, M. Bejaoui, S. Ben Hassine, W. Chouk, A. Oueslati, W. Oueslati, Multifunctional chitosan/montmorillonite/TiO_2 nanocomposites: correlating microstructure with dielectric and photocatalytic properties, *Journal of the Indian Chemical Society*, 2025, **102**, 101606, doi: 10.1016/j.jics.2025.101606.

[18] Y. Liu, X. Zhao, J. Yin, Enhanced electro-responsive electrorheological efficiency of polyethylene oxide-intercalated montmorillonite nanocomposite suspension, *Colloids and Surfaces A: Physicochemical and Engineering Aspects*, 2023, **666**, 131239, doi: 10.1016/j.colsurfa.2023.131239.

[19] Shobhna Choudhary, Priyanka Dhatarwalb and R J Sengwab, Study on crystalline phases and degree of crystallinity of the melt compounded PVA/MMT and PVA/PVP/MMT nanocomposites, *Indian Journal of Pure & Applied Physics*, 2021, **59**, 92-102, doi: 10.56042/ijpap.v59i2.45457.

[20] M. F. Hossain, T. C. Paul, M. N. I. Khan, S. Islam, P. Bala, Magnetic and dielectric properties of $ZnFe_2O_4$/nanoclay composites synthesized *via* Sol-gel autocombustion, *Materials Chemistry and Physics*, 2021, **271**, 124914, doi: 10.1016/j.matchemphys.2021.124914.

[21] R. J. Sengwa, C. P. Charan, Radio frequencies dielectric and electrical properties of nanomaterial-in-polymer-in-nanomaterial based PMMA/OMMT composites, *Materials Letters*, 2025, **400**, 139157, doi: 10.1016/j.matlet.2025.139157.

[22] H.-Y. Yao, Y.-W. Lin, T.-H. Chang, Dielectric properties of $BaTiO_3$–epoxy nanocomposites in the microwave regime, *Polymers*, 2021, **13**, 1391, doi: 10.3390/polym13091391.

[23] Y. Zhang, B. Ma, X. Jia, Preparation and characterization of novel MP-MMT/PMMA composite microspheres, *Journal of Dispersion Science and Technology*, 2024, **45**, 2028-2036, doi: 10.1080/01932691.2023.2245450.

[24] X.-H. Zhang, C.-Y. Wei, L.-L. Zha, J.-W. Chen, J.-W. Wang, H.-L. Yu, J.-H. Wu, Facile one-pot synthesis of polypyrrole-coated magnetic montmorillonite for enhanced microwave absorption and sunlight-induced heat generation, *Journal of Alloys and Compounds*, 2024, **971**, 172676, doi: 10.1016/j.jallcom.2023.172676.

[25] Y. Wang, Y. Cheng, C. Yin, J. Zhang, X. Zhang, J. Zhang, Seashell-inspired switchable waterborne coatings with complete biodegradability, intrinsic flame-retardance, and high transparency, *ACS Nano*, 2023, **17**, 12433-12444, doi: 10.1021/acsnano.3c01866.
[26] L. Su, C. Fang, H. Luo, Functionalized montmorillonite/epoxy resin nanocomposites with enhanced thermal and mechanical properties, *RSC Advances*, 2024, **14**, 31251-31258, doi: 10.1039/d4ra03125c.
[27] L. G. Li, G.-H. Zhang, A. K. H. Kwan, Exploring submarine 3D printing: enhancing washout resistance and strength of 3D printable mortar, *Journal of Materials in Civil Engineering*, 2025, **37**, 04025019, doi: 10.1061/jmcee7.mteng-19089.